

**FLUID-STRUCTURE INTERACTION ANALYSIS
ON AIRCRAFT WING INTERGRATED WITH
WING TIP DEVICE**

TAN YAO BIN

**SCHOOL OF AEROSPACE ENGINEERING
UNIVERSITI SAINS MALAYSIA
2021**

**FLUID-STRUCTURE INTERACTION ANALYSIS OF AIRCRAFT WING
INTEGRATED WITH WING TIP DEVICE**

by

TAN YAO BIN

**Thesis submitted in fulfilment of the requirements for the
Bachelor Degree of Engineering (Honours) (Aerospace Engineering)**

June 2021

ENDORSEMENT

I, Tan Yao Bin hereby declare that all corrections and comments made by the supervisor and examiner have been taken consideration and rectified accordingly.



(Signature of Student)

Date: 25/ 06/ 2021



(Signature of Supervisor)

Name: Dr. Mohammad Hafifi Hafiz

Date: 10.7.2021



(Signature of Examiner)

Name: Dr. Chang Wei Shyang

Date: 10/07/2021

DECLARATION

This thesis is the result of my own investigation, except where otherwise stated and has not previously been accepted in substance for any degree and is not being concurrently submitted in candidature for any other degree.



(Signature of Student)

Date: 25/ 06/ 2021

ACKNOWLEDGEMENTS

Firstly, I express my thanks to the Almighty God for His showers of blessings throughout my research work to complete my Final Year Project (FYP).

Besides my weary efforts, I would like to express my deepest gratitude to the individuals who assisted and supported me during the lassitude of my research work.

Furthermore, I express my deep appreciation to my research supervisor Dr. Mohammad Hafifi Hafiz Bin Ishaik for offering me the opportunity to do research on this title and provide me with invaluable guidance and positive support throughout the research, as well as having the faith in me during my research work. It was a great experience and honour to work under Dr Hafifi guidance. I pay my sincere gratitude to my examiner, Dr Chang Wei Shyang for his advice and suggestion throughout my research. A very special gratitude goes out to Assoc. Prof. Dr. Farzad Ismail and the CFD team member for sharing their wealth CFD knowledge and expertise in FSI.

Moreover, I would like to express my appreciation to the FYP coordinator Dr. Aslina Anjang Ab Rahman for the guideline in preparing the thesis. I would like to acknowledge school of Aerospace engineering for the support in computational resources and software for completing this project. Special thanks to Mrs. Rahayu bt. Dorahim Abdul Rahim for her valuable assistance in providing the computation resources and assistance during software and hardware problem occurs.

ABSTRACT

Wing tip device is a common device nowadays on an aircraft to improve the aerodynamic performance of the aircraft. Wing tip device's purpose is usually to reduce the induced drag by diminishing the downwash of the flow around the wing tip. The optimal design to improve the aerodynamic performance of wing tip and the fluid-structure interaction (FSI) effect on the aircraft wing is still a wide field to be discovered and should be studied in an ample scope. This report is carried out to study the aerodynamic performance of the designed blended split wing tip along with comprehending the study of FSI analysis to investigate the structural deformation and stresses on the wing integrated with wing tip device. The research is conducted in a subsonic and transonic region with speed varies from 0.2 Ma to 0.6 Ma. Thereafter, the aerodynamic analysis is performed at 0° angle of attack (AOA) to 16° angle of attack at 0.2 Mach. Numerical method of 3D Computational Fluid Dynamics (CFD) analysis is used to analyze the aerodynamic performance of the proposed split wing tip design and comparison is done to justify the improvement. Besides, 2D aerodynamic analysis is used to validate and comprehend the 3D CFD analysis. A total of 3 wings with no wing tip, split wing tip and blended split wing tip is analyzed using ANSYS CFD. To inspect the structural stresses on the wing, a one-way FSI approach is included in this report. The structural stress at the wing root, mid-span area and wing tip is studied and compared between the three wing models at different Mach number and angle of attack. The finding indicates that the proposed blended split wing tip design have a drawback in aerodynamic performance at Mach number of 0.2, 0.4 and 0.6. However, this wing tip design benefits the aerodynamic performance when AOA is varying from 0 to 16 while Mach number is maintained at 0.2. It has an overall increase of 6.684% in the aerodynamic performance when compared with wing with no wing tip. From the structural point of view, the

blended split wing tip device can relieve the high concentrated stress in the stress raiser to a preferred region in the top winglet.

ABSTRAK

Peranti hujung sayap adalah alat yang biasa digunakan pada pesawat untuk meningkatkan prestasi aerodinamik pesawat pada zaman kini. Peranti hujung sayap biasanya dipasang untuk mengurangkan daya seret dengan mengurangkan aliran menurun di sekitar hujung sayap. Reka bentuk yang optimum untuk meningkatkan prestasi aerodinamik hujung sayap dan kesan interaksi struktur bendalir (FSI) pada sayap pesawat adalah bidang yang luas untuk ditemui dan harus dikaji dalam ruang lingkup yang luas. Laporan ini dilakukan untuk mengkaji prestasi aerodinamik peranti hujung sayap yang dicadang dan menjalankan kajian FSI untuk menyiasat ubah bentuk struktur dan tekanan pada sayap yang disepadukan dengan peranti hujung sayap. Penyelidikan dilakukan dengan meniru keadaan sebenar di mana sayap bergerak di kawasan subsonik dan transonik dengan kelajuan bervariasi dari 0.2 Ma hingga 0.6 Ma. Selepas itu, analisis aerodinamik dilakukan pada sudut aliran udara (AOA) 0° hingga sudut 16° pada 0.2 Mach. Kaedah analisis 3D Pengiraan Dynamic Bendalir (CFD) digunakan untuk menganalisis prestasi aerodinamik reka bentuk hujung sayap yang dicadangkan dan perbandingan dilakukan untuk menbandingkan prestasi peningkatan. Selain itu, analisis aerodinamik 2D digunakan untuk mengesahkan dan memahami analisis CFD 3D. Sebanyak 3 sayap yang dipasang dengan peranti hujung sayap yang berbeza akan dianalisis menggunakan ANSYS CFD. Untuk memeriksa tekanan struktur di sayap, pendekatan FSI sehalu dimasukkan dalam laporan ini. Tekanan struktur di akar sayap, kawasan pertengahan sayap dan hujung sayap akan dikaji dan dibandingkan antara tiga model sayap. Kajian akan dibuat dengan bilangan Mach dan sudut aliran udara yang berbeza. Hasil kajian menunjukkan bahawa reka bentuk hujung sayap yang dicadangkan mempunyai kelemahan dalam prestasi aerodinamik pada bilangan Mach 0,2, 0,4 dan 0,6. Walau bagaimanapun, reka bentuk hujung sayap ini menguntungkan prestasi

aerodinamik apabila AOA berbeza dari 0 hingga 16 sementara bilangan Mach dikekalkan pada 0.2. Ia mempunyai peningkatan keseluruhan dalam prestasi aerodinamik sebanyak 6.684% jika dibandingkan dengan sayap tanpa hujung sayap. Dari sudut pandangan struktur, peranti hujung sayap yang dicadang dapat menghilangkan tekanan yang tinggi pada lokasi penambah tekanan ke sayap atas pada peranti hujung sayap.

TABLE OF CONTENTS

| | |
|--|--------------|
| ENDORSEMENT..... | III |
| DECLARATION | IV |
| ACKNOWLEDGEMENTS..... | V |
| ABSTRACT | VI |
| ABSTRAK | VIII |
| TABLE OF CONTENTS | X |
| LIST OF FIGURES..... | XIII |
| LIST OF TABLES..... | XVIII |
| LIST OF ABBREVIATIONS..... | XX |
| LIST OF SYMBOLS..... | XXI |
| CHAPTER 1 INTRODUCTION | 1 |
| 1.1 General Overview | 1 |
| 1.2 Problem Statement | 2 |
| 1.3 Research Objectives | 3 |
| 1.4 Research Scope | 4 |
| 1.5 Thesis Outline | 4 |
| CHAPTER 2 LITERATURE REVIEW | 6 |
| 2.1 CFD in Predicting Aerodynamic Forces | 6 |
| 2.2 Aerodynamic of Wing Tip Device | 7 |
| 2.3 Aerodynamic of Split Wing Tip Device..... | 9 |
| 2.4 Selection of Turbulent Model | 10 |
| 2.5 Design of Proposed Wing Tip Device | 12 |
| 2.6 Fluid-Structure Interaction..... | 15 |

| | | |
|------------------|--|-----------|
| CHAPTER 3 | METHODOLOGY..... | 18 |
| 3.1 | Overview..... | 18 |
| 3.2 | 3D Aerodynamic Analysis..... | 20 |
| 3.2.1 | 3D Wing Model CAD Design | 20 |
| 3.2.2 | Design Parameter of 3D Wing..... | 24 |
| 3.2.3 | 3D Fluid Domain Geometry Setup | 25 |
| 3.2.4 | 3D Meshing Grid Independent Test..... | 27 |
| 3.2.5 | 3D Fluid Domain Meshing Set Up | 29 |
| 3.2.6 | Estimation of Thickness of First Inflation Layer..... | 34 |
| 3.2.7 | Numerical Solution Solver Set Up..... | 35 |
| 3.2.8 | Reference Values for Solver..... | 37 |
| 3.2.9 | Process of Result Validation with NACA 4412 Wing Model..... | 38 |
| 3.3 | 2D Aerodynamic Analysis..... | 42 |
| 3.3.1 | 2D Fluid Domain Geometry Setup | 42 |
| 3.3.2 | 2D Fluid Domain Meshing Setup | 43 |
| 3.3.3 | 2D Meshing Grid Independent Test..... | 44 |
| 3.3.4 | 2D Numerical Solver Set Up..... | 46 |
| 3.4 | Fluid-Structure Interaction (FSI)..... | 46 |
| 3.4.1 | One-Way Coupling FSI with Steady State CFD Analysis | 47 |
| CHAPTER 4 | RESULTS AND DISCUSSION | 53 |
| 4.1 | Aerodynamic Analysis | 53 |
| 4.1.1 | 3D NACA 4412 Wing Model Result Validation..... | 53 |
| 4.1.2 | Effect of Mach Number on Aerodynamic Performance of the 3D Wing Model with Different Type of Wing Tip..... | 55 |
| 4.1.3 | Effect of Mach Number on C_l | 58 |
| 4.1.4 | Effect of Mach Number on C_d | 59 |
| 4.1.5 | Effect of Angle of Attack on the Aerodynamic performance of 3D Wing Model with Different Type of Wing Tip..... | 62 |

| | | |
|--|---|------------|
| 4.1.6 | Effect of Angle of Attack on C_l | 66 |
| 4.1.7 | Effect of Angle of Attack on C_d | 69 |
| 4.1.8 | C_l and C_d Simulation Convergence Plots | 72 |
| 4.1.9 | Effect of Angle of Attack to the Velocity Flow Contour..... | 77 |
| 4.1.10 | Solution Quality in 2D Analysis | 78 |
| 4.1.11 | Solution Quality for 3D Analysis | 80 |
| 4.1.12 | Static Pressure Contour for 3D Wing Model with Different Type of Wing Tip when varying Mach Number..... | 80 |
| 4.1.13 | Static Pressure Contour for 3D Wing Model with Different Type of Wing Tip When Varying Angle of Attack..... | 83 |
| 4.2 | Fluid Structure Interaction Analysis..... | 87 |
| 4.2.1 | Simulation Result of Structural Response with respect to Mach Number 87 | |
| 4.2.2 | Simulation Result of Structural response with respect to Angle of Attack 97 | |
| CHAPTER 5 CONCLUSIONS AND RECOMMENDATIONS..... | | 105 |
| 5.1 | Conclusion | 105 |
| 5.2 | Recommendations for Future Research..... | 106 |
| REFERENCES | | 108 |
| APPENDICES | | 110 |
| A: Detail drawing of 3D wing model with wing tip device design (All dimensions are in millimeters) | | 111 |
| B: Fluid Domain Control Volume Set Up | | 114 |
| C: 3D Fluid Domain Meshing Set Up | | 116 |
| D: 3D Aerodynamic Solver Set Up..... | | 117 |
| E: 2D Fluid Domain Meshing Set Up | | 119 |
| F: 2D Numerical Solver Set Up | | 121 |
| G: FEA Meshing Set Up..... | | 123 |

LIST OF FIGURES

| | |
|---|----|
| Figure 1.1: Split wing tip design of Boeing 737 max..... | 1 |
| Figure 2.1: Estimation of reduction in induced drag and total drag at Mach 0.78 and lift coefficient of 0.51 on blended winglet of 737-800 relative to 737-800 without winglet..... | 7 |
| Figure 2.2: Formation of wing tip vortices | 8 |
| Figure 2.3: Lift vector of split wing tip | 9 |
| Figure 2.4: Drag polar of wing with and without split wing tip | 10 |
| Figure 2.5: Induced drag of several wing lifting surface according to Trefftz-plane theory | 13 |
| Figure 2.6: The streamwise pressure distributions over the upper surface of the wing for different winglet configurations: (a) wingtip without winglet, (b) winglet with sharp corner, (c) blended winglet..... | 14 |
| Figure 2.7: Effect of winglet cant angle on lift to drag ratio | 15 |
| Figure 3.1: Overall project flow chart | 19 |
| Figure 3.2: Flow chart of one-way coupling FSI | 20 |
| Figure 3.3: The side, top and isometric view of airfoil profile at specific location for 3D wing design | 21 |
| Figure 3.4: Top, isometric, front and side view of split wing tip wing design | 22 |
| Figure 3.5: Top, isometric, front and side view of wing design with no wing tip | 23 |
| Figure 3.6: Guidelines for blended split wing tip design | 24 |
| Figure 3.7: Top, isometric, front and side view of blended split wing tip wing design | 24 |
| Figure 3.8: Width of fluid flow domain..... | 26 |
| Figure 3.9: Dimensions of fluid flow domain..... | 27 |
| Figure 3.10: FLUENT GIT graph | 28 |

| | |
|---|----|
| Figure 3.11: Symmetry, isometric and zoom view of the 3D mesh set up..... | 31 |
| Figure 3.12: Inflation layer in the wall boundary layer | 32 |
| Figure 3.13: Named selection for boundary conditions | 32 |
| Figure 3.14: Volume of the mesh cells..... | 33 |
| Figure 3.15: The planform area for wing with wing tip | 37 |
| Figure 3.16: Reference value for solver | 38 |
| Figure 3.17: Wing model of NACA 4412 rectangular wing | 39 |
| Figure 3.18: Graph of lift coefficient versus angle of attack at $3e^6$ Re. (Petinrin & Onoja, 2017) | 40 |
| Figure 3.19: Graph of lift coefficient versus angle of attack at varying Reynolds numbers (Petinrin & Onoja, 2017)..... | 40 |
| Figure 3.20: C-type fluid domain for 2D airfoil | 43 |
| Figure 3.21: Mesh set up for 2D airfoil | 43 |
| Figure 3.22: Named selection for boundary condition of 2D airfoil..... | 44 |
| Figure 3.23: 2D FLUENT GIT result..... | 45 |
| Figure 3.24: One-way coupling FSI setup | 47 |
| Figure 3.25: Comparison of strength to weight ratio of Aluminium with other materials..... | 48 |
| Figure 3.26: Material assigned to the geometry | 49 |
| Figure 3.27: Fixed support boundary condition..... | 49 |
| Figure 3.28: Mesh set up in the wing with wing tip device | 50 |
| Figure 3.29: Sphere of influence created to refine the mesh | 50 |
| Figure 3.30: Refined mesh at the wing tip device..... | 50 |
| Figure 3.31: Mapping surface with imported pressure load from CFD | 52 |
| Figure 3.32: Imported load transfer summary | 52 |
| Figure 4.1: Graph of lift coefficient versus angle of attack for NACA 4412 rectangular wing by analytical calculation | 54 |

| | |
|---|----|
| Figure 4.2: Variation of lift coefficient with Mach number for different type of wing tip device..... | 56 |
| Figure 4.3: Variation of drag coefficient with Mach number for different type of wing tip device | 57 |
| Figure 4.4: The pressure contour for Mach number 0.2, 0.4 and 0.6 respectively | 59 |
| Figure 4.5: Wall shear stress against the position along the airfoil at Mach number of 0.2, 0.4 and 0.6 respectively. | 61 |
| Figure 4.6: The effect of fluid flow velocity to the drag coefficient according to Juniper, (2015) | 62 |
| Figure 4.7: Variation of lift coefficient with angle of attack for wing with different type of wing tip device | 64 |
| Figure 4.8: Variation of drag coefficient with angle of attack for wing with different type of wing tip device | 64 |
| Figure 4.9: The area between the curves of pressure coefficient over the upper and lower surfaces of an airfoil is the lift coefficient (John D. Anderson, 1989)..... | 67 |
| Figure 4.10: Pressure Coefficient against chord length from AOA=2°, 4°, 6°, 8°, 10°, 14° and 16° respectively | 68 |
| Figure 4.11: Wall shear stress against the position along the airfoil at AOA of 8°, 10°, 12° and 14° and 16° respectively..... | 71 |
| Figure 4.12: Cl iteration plot for wing with no wing tip for 8°, 10°, 12°, 14° and 16° AOA respectively. | 72 |
| Figure 4.13: Cd iteration plot for wing with no wing tip for 8°, 10°, 12°, 14° and 16° AOA respectively. | 73 |
| Figure 4.14: Cl iteration plot for wing with split wing tip for 8°, 10°, 12°, 14° and 16° AOA respectively..... | 74 |
| Figure 4.15: Cd iteration plot for wing with split wing tip for 8°, 10°, 12°, 14° and 16° AOA respectively..... | 75 |
| Figure 4.16: Cl iteration plot for wing with blended split wing tip for 8° and 10° AOA respectively | 76 |

| | |
|---|----|
| Figure 4.17: Cd iteration plot for wing with blended split wing tip for 8° and 10° AOA respectively. | 76 |
| Figure 4.18: Velocity flow contour at angle of attack of 10°, 12°, 14° and 16° respectively. | 77 |
| Figure 4.19: Quadrilateral mesh near the 2D airfoil | 79 |
| Figure 4.20: Wall y+ value for the 2D airfoil | 79 |
| Figure 4.21: Wall y+ value around the 3D wing model | 80 |
| Figure 4.22: Static pressure distribution on wing with no wing tip at Mach numbers of 0.2, 0.4 and 0.6 respectively | 81 |
| Figure 4.23: Static pressure distribution on wing surface integrated with split wing tip at Mach number of 0.2, 0.4 and 0.6 respectively. | 82 |
| Figure 4.24: Static pressure distribution on wing surface integrated with blended split wing tip at Mach number of 0.2, 0.4 and 0.6 respectively | 82 |
| Figure 4.25: Static pressure distribution on wing with no wing tip at Mach number of 0.2 and AOA of 2°, 4°, 6°, 8°, 10°, 12°, 14° and 16° respectively... | 83 |
| Figure 4.26: Static pressure distribution on wing with split wing tip at Mach number of 0.2 and AOA of 2°, 4°, 6°, 8°, 10°, 12°, 14° and 16° respectively... | 84 |
| Figure 4.27: Static pressure distribution on wing with blended split wing tip at Mach number of 0.2 and AOA of 2°, 4°, 6°, 8°, 10°, 12° and 14° respectively | 85 |
| Figure 4.28: The equivalent Von Mises stress at the wing root, mid span area and wing tip of wing with blended split wing tip at Mach number of 0.2, 0.4 and 0.6 respectively | 88 |
| Figure 4.29: The equivalent Von Mises stress at the wing root, mid span area and wing tip of wing with split wing tip at Mach number of 0.2, 0.4 and 0.6 respectively | 89 |
| Figure 4.30: The equivalent Von Mises stress at the wing root, mid span area and wing tip of wing with no wing tip at Mach number of 0.2, 0.4 and 0.6 respectively | 90 |

| | |
|--|-----|
| Figure 4.31: Graph of maximum equivalent stress at wing root against Mach number | 91 |
| Figure 4.32: Installation of winglet that induce a growth in maximum spanwise stress. (Gueraiche & Popov, 2017)..... | 93 |
| Figure 4.33: Graph of maximum equivalent stress at wing tip against Mach number | 94 |
| Figure 4.34: Graph of maximum total deformation against Mach number | 96 |
| Figure 4.35: The equivalent Von Mises stress at the wing root, mid span area and wing tip of wing with blended split wing tip at AOA of 4, 6, and 8 respectively | 97 |
| Figure 4.36: The equivalent Von Mises stress at the wing root, mid span area and wing tip of wing with split wing tip at AOA of 4, 6, and 8 respectively | 98 |
| Figure 4.37: The equivalent Von Mises stress at the wing root, mid span area and wing tip of wing with no wing tip at AOA of 4, 6, and 8 respectively | 99 |
| Figure 4.38: Graph of maximum equivalent stress at wing root against angle of attack..... | 100 |
| Figure 4.39: Maximum Von Mises stress on wing with different winglet varies with angle of attack (Gueraiche & Popov, 2017) | 101 |
| Figure 4.40: Graph of maximum equivalent stress at wing tip against angle of attack | 103 |
| Figure 5.1: The dimension setting and value for the fluid flow domain | 114 |
| Figure 5.2: The dimensions of refined domain | 114 |
| Figure 5.3: Refined domain control volume | 115 |

LIST OF TABLES

| | |
|---|----|
| Table 3.1: Basic design parameter of 3d wing | 25 |
| Table 3.2: FLUENT GIT result..... | 28 |
| Table 3.3: Mesh quality of fluid domain | 33 |
| Table 3.4: Mesh quality of 2D fluid domain..... | 44 |
| Table 3.5: 2D FLUENT GIT result | 45 |
| Table 3.6: Mechanical properties of aluminium | 48 |
| Table 3.7: Structure 3D mesh quality | 51 |
| Table 4.1: Table of lift coefficient of NACA 4412 rectangular wing by analytical calculation and simulation at Reynolds number of $13e^6$ | 54 |
| Table 4.2: Lift coefficient and drag coefficient for different wing tip device at various Mach number | 55 |
| Table 4.3: Drag Polar for different wing tip device at various Mach number..... | 56 |
| Table 4.4: The variation of pressure difference between upper and lower airfoil as the Mach number increases..... | 59 |
| Table 4.5: Value of wall shear stress and the point of flow detachment | 61 |
| Table 4.6: Lift coefficient and drag coefficient for wing with different wing tip device at various angle of attack | 63 |
| Table 4.7: Drag Polar for wing with different wing tip device at various angle of attack..... | 63 |
| Table 4.8: Maximum equivalent stress at wing root of the wing with different wing tip device at different Mach number | 91 |
| Table 4.9: The maximum equivalent stress at mid span area of each wing with different wing tip device and the growth in equivalent stress at the mid span area due to wing tip installation | 92 |
| Table 4.10: The maximum equivalent stress at wing tip for both wing with blended split wing tip and split wing tip at different Mach number. | 93 |

| | |
|---|-----|
| Table 4.11: The maximum deformation of the wing with different wing tip device at different Mach number | 95 |
| Table 4.12: Maximum equivalent stress at wing root of the wing with different wing tip device at different angle of attack | 100 |
| Table 4.13: The maximum equivalent stress at mid span area of each wing with different wing tip device and the growth in equivalent stress at the mid span area due to wing tip installation at different AOA | 102 |
| Table 4.14: The maximum equivalent stress at wing tip for both wing with blended split wing tip and split wing tip at different angle of attack. | 103 |
| Table 5.1: 3D fluid domain meshing set up | 116 |
| Table 5.2: The solver setup when Mach = 0.2 and AOA = 12° | 117 |
| Table 5.3: 2D Fluid Domain Meshing Set Up | 119 |
| Table 5.4: The solver setup of 2D airfoil when Mach= 0.2 and AOA= 12° | 121 |
| Table 5.5: Meshing set up (FEA) | 123 |

LIST OF ABBREVIATIONS

| | |
|------|---|
| AOA | Angle of attack |
| CAD | Computer Aided Design |
| CFD | Computational fluid dynamics |
| CPU | Central processing unit |
| FEA | Finite element analysis |
| FSI | Fluid-structure interaction |
| GIT | Grid Independent Test |
| NACA | National Advisory Committee for Aeronautics |
| RAM | Random-access memory |
| RANS | Reynolds-Averaged Navier Stokes |
| SA | Spalart-Allmaras |
| SST | Shear-stress Transport |

LIST OF SYMBOLS

| | |
|--------------|---|
| $k-\epsilon$ | k-epsilon |
| $k-\omega$ | k-omega |
| C | Chord length [m] |
| Re | Reynolds number |
| Δy | First layer thickness of boundary layer mesh [m] |
| μ | Dynamic viscosity of fluid [Ns/m ²] |
| v | Velocity of fluid [m/s ²] |
| ρ | Density of fluid [kg/m ³] |
| U_T | Frictional velocity [m/s ²] |
| τ_w | Wall shear stress [Pa] |
| L | Characteristic length of the wing in the direction of chord [m] |
| C_f | Skin friction coefficient |
| a | Lift slope of finite wing |
| a_0 | Lift slope of infinite wing |
| e | Span efficiency factor |
| AR | Aspect ratio of finite wing |
| π | Pi |
| α | Angle of attack |
| C_L | Lift coefficient |
| C_D | Drag coefficient |

| | |
|-------|---------------------------------|
| ν | Poisson ratio |
| S_y | Yield strength [MPa] |
| S_u | Ultimate tensile strength [MPa] |
| E | Modulus of elasticity [GPa] |

CHAPTER 1

INTRODUCTION

1.1 General Overview

Boeing 737 MAX is the latest Boeing 737 series plane. Boeing 737 max took its first flight in early of 2016. One of the important modifications done on it is the aerodynamic changes of its split wing tip design as shown in Figure 1.1. Wing tip device is a very common device to increase the aerodynamic performance of a fixed-wing subsonic and transonic aircraft.

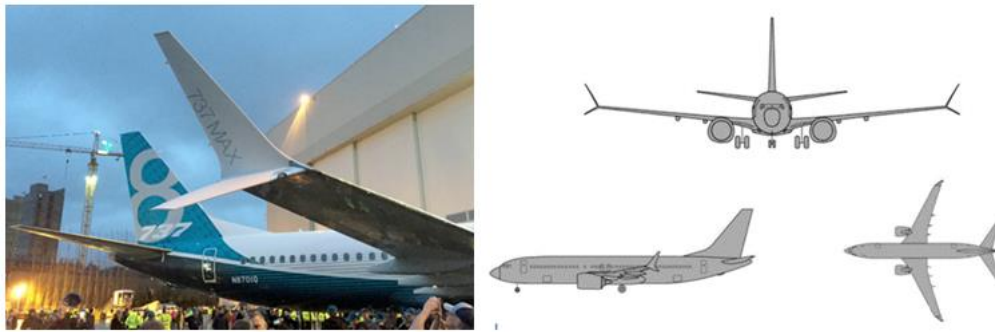


Figure 1.1: Split wing tip design of Boeing 737 max

Most of the fuel-efficient aircraft nowadays is integrated with wing tip device. The most important function of the wing tip device is its intended effect to ease the aircraft drag. Hossain et al., (2011) deduced that wing tip devices can reduce the lift induced drag by approximately 10% to 15% if the wing tip device is integrated into the wing. Over the year, the field of study aerodynamic behaviour of a wing tip device has become a general mainstream for researcher, designer and manufacturer. The aerodynamic flow study on a fixed-wing with wing tip device indeed possesses vital importance to investigate its aerodynamic performance at the subsonic and transonic flow. Besides, the optimized wing tip device is necessary to be installed on an aircraft wing to fulfil the improvement in fuel efficiency and minimize fuel consumption. This

investigation of external aerodynamic flow over the wing can be done in wind tunnel test or using CFD numerical simulation.

It is undeniable aerodynamic flow study over the wing with wing tip device is crucial to the aerospace industry to determine the aerodynamic force acting on the wing so that improvement in lift to drag ratio can be done and increase the efficiency. However, the pressure distribution as the fluid flow through the wing will impose a static loading to the wing structure as well. Hence, it is also critical to realize the effect of the structural forces imposed on the wing structure.

All in all, the FSI analysis which composed of aerodynamic analysis along with structural analysis will serve as a tool to effectively evaluate the wing model integrated with wing tip device at subsonic and transonic speed. This thesis presents the overview design along with the FSI analysis of the wing integrated with wing tip device.

1.2 Problem Statement

Over the years, there are some aerodynamic analyses performed to prove the benefit of integrating wing tip devices to improve the aerodynamic performance of a wing. The aerodynamic analysis is insufficient to support the analysis of these design. Comprehensive studies about how the stress develops in wing structure with a winglet when pressure distribution exerted on it should be carried out. In order to overcome this problem, this study offered analysis of the performance of a wing with wing tip device with coupling both of the fluid and structure. To be more precise, the pressure distribution on the wing surface may deform the wing winglet structure and the deformation on the wing structure will lead to an altering of initial pressure distribution and create a new pressure distribution. This new pressure distribution is then used to compute the deformation of the wing structure in the next iteration. Two-way FSI will need to be

carried out if the deformation of the wing that leads to a change in the fluid pressure and further results in a lift and drag change is to be studied. However, to simplify the complexity of the analysis problem only one-way FSI is conducted.

The severe deformation of the wing installed with winglet might lead to a detrimental effect on the flow field and should be avoided. If a wing is loaded with very high flexural strength, undesirable structure failure is exacerbated on the wing. This research will be performed with a fluid-structure interaction method to study the best performance of the wing that install with winglet. This analysis is carried out in the subsonic and transonic region.

There is no precise or best solution for the wing tip design as all wing tip device has its function in different manners. Hence, the optimal solution on the aerodynamic design of the wing tip and the FSI effect on the wing is still obscure. This research will present a new proposed prototype design of wing tip and investigate its aerodynamic performance to offer a humble effort to support the development of future wing tip device in the aircraft industry.

1.3 Research Objectives

The final aims of this thesis are:

1. To determine the aerodynamic performance of the designed wings installed with wing tip device using numerical approach.
2. To study the structural response of the wings installed with wing tip devices through numerical study of Fluid Structure interaction (FSI) analysis.

1.4 Research Scope

The study hereinabove this thesis is solely numerical simulation work. The actual fabrication of the 3D wing model and the experimental work is excluded. This study is a preliminary approach to study the aerodynamic performance and FSI of a new wing tip prototype. The aerodynamic performance of this new wing tip design prototype is studied using CFD simulation. In the study of aerodynamic performance, only the altitude at 30000ft is considered. Hence, the density, pressure, Mach number and viscosity of the air at this altitude will be used in the simulation. The performance of the wing tip device varying from subsonic to transonic speed is studied. Besides, numerical simulation of a different angle of attack from 0° to 16° is analysed. The flow around the external wing-body undergoes laminar to turbulent transition. However, the transition happened at the very beginning of the wing chord. Hence, only turbulent flow around the external wing body is considered. The heat transfer in the flow is negligible. In the static structural simulation, the material selection is Aluminium alloy as it is the conventional material used in most aircraft wing. Lastly, the stress of the wing is focused.

1.5 Thesis Outline

Chapter 1 in this thesis is related to the introduction of the Boeing 737 max wing tip device and its benefit in terms of aerodynamic performance. The highlight of this study including problem statement, research objectives and research scope is comprehended in Chapter 1. Chapter 2 mentioned the literature findings on the relevant study in the past related to aerodynamic performance of wing tip, numerical simulation of CFD, FSI and the optimized wing tip design. Chapter 3 on the other hand is about the methodology carried out to achieve the result. Chapter 3 is mainly divided into 3D CFD analysis of wing models and the one-way FSI approach in steady state. Chapter 4 is the

result and discussion part. The results obtained are presented and discussed. The study is concluded with a contribution of knowledge and recommendations in Chapter 5.

CHAPTER 2

LITERATURE REVIEW

2.1 CFD in Predicting Aerodynamic Forces

In general, the aerodynamic forces are lift and drag. The profile drag can be further distributed into skin friction drag and pressure drag. The skin friction drag can be treated as the drag caused by the viscous effect (viscosity and turbulence) when air flow through the surface of the wing. The pressure drag is a very complicated drag that is described by the flow mechanism of air particle through the wing. The pressure drag includes the study of viscous effect, shock, flow separation and attached flow (Lean, 2005). The lift induced drag, on the other hand, is the result of perturbation of pressure distribution due to the formation of wing tip vortices. Lean, (2005) claimed that the study of drag is carried out by Computational Fluid Dynamics (CFD) methods based on Euler and Navier Stokes equations. In fact, CFD also helps to predict the entire flow field around the wing in detail. Lean, (2005) also presented the Trefftz-plane theory to evaluate the induced drag of the wing. He estimated the percentage reduction of induced drag and total drag at Mach 0.78 and lift coefficient of 0.51 due to blended winglet on 737-800 relative to a 737-800 without winglet using Trefftz-plane theory and CFD analysis. The results were then compared with Boeing flight test as shown in Figure 2.1. The result shows that CFD method estimates the reduction in induced drag more accurately than the Trefftz-plane theory. The percentage of total drag reduction estimated by CFD agrees reasonably well with the actual experimental flight test result.

| Component | Drag reduction, % of total AP |
|--|-------------------------------|
| Ideal based on Trefftz-plane configuration only: Induced drag | 4.8 |
| High-fidelity CFD (TRANAIR) based on actual wing shape with estimated 1-g aeroelastic deflections: Induced drag Total drag | 3.1 2.8 |
| Inferred from average of Boeing flight-test measurements: Total drag | 3.2 |

Figure 2.1: Estimation of reduction in induced drag and total drag at Mach 0.78 and lift coefficient of 0.51 on blended winglet of 737-800 relative to 737-800 without winglet.

Ishak et al., (2020) used Computation Fluid Dynamic (CFD) FLUENT simulation to solve the compressible Navier Stokes equations to analyze the Ruppell Griffon Vulture (RGV) type winglet. The compressible Navier Stokes equations which hold conservation of mass, conservation of momentum and conservation of energy are to be solved at each control volume boundary. The CFD is utilized to solve the compressible Navier Stokes equations by means of using Reynolds-Averaged-Navier-Stokes (RANS) turbulent modelling based on SST $k-\omega$ model. The RANS equations and the turbulent transport equations are solved with second order limited finite volume method (FVM) of Roe's flux differencing approach and implicit time discretization. Milic, (2020) used ANSYS CFD with k - ω SST turbulence model to study the aerodynamic performance of wing with and without split wing tip.

2.2 Aerodynamic of Wing Tip Device

Wing tip vortices is a spiral circulatory motion of air that trails behind the wing tip and represent energy loses. Wing tip vortices are caused by the air beneath the wing flow over the wing tip to the top of the wing as there is pressure difference across the wing surfaces when air is flowing through (John D. Anderson, 1989). As a result, wing tip vortices create downwash and result in lift induced drag. Figure 2.2 illustrated the formation of wing tip vortices.

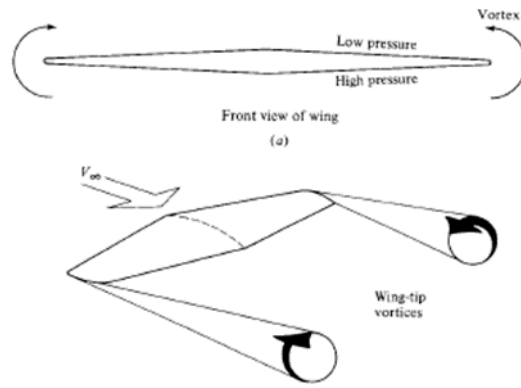


Figure 2.2: Formation of wing tip vortices

The aerodynamic efficiency is usually improved through the installation of wing tip device. The effect of wing integrated with wing tip device is the wing tip flow is diffused and hence result in reducing the wing tip vortices of aircraft. Sometimes the winglet is twisted to create a rotating vortex flow with a forward component at the wing tip. This forward component force is a form of “negative drag” and act to reduce the total wing drag. (Hossain et al., 2011)

Based on Ishak et al., (2020), winglet is used to alter the flow of trailing tip vortex of the wing. Winglet nowadays plays an important role to reduce the induced drag and furthermore improve flight efficiency as well. The reason behind it is winglet tries to restore energy in the wing tip vortex by diffused out the strength of wing tip vortex. The reduction of the strength of wing tip vortex is mainly to ease the downwash and the lift induced drag created by assisting in restoring the energy loss in wingtip vortices. The addition of a wing tip device intentionally increases the wing tip surface and the purpose of smoothing the flow vortices in the tip can be achieved. In the meantime, the lift generated at the wingtip also increases as the downwash decreases.

The induced drag reduction by adding wingtip device is usually detriment by an increase in other drag component. Owing to the fact that, adding of wingtip device increase the wetted surface area and further increase the skin friction drag and pressure

drag. There is also unfavourable pressure distributions and pressure gradient at the area of connection between wing and winglet that may increase the profile drag. Hence, the wingtip device must be effective to decrease the lift induced drag to balance out these detriment effects.

2.3 Aerodynamic of Split Wing Tip Device

Boeing claimed that with the former blended winglet design, the airflow around the tip is altered to create lift but primarily vectored toward the fuselage besides reducing the lift induced drag. By installing the split wing tip device, the lift vectored toward the fuselage is balanced by the lift vectored away through introducing the lower aerofoil on the blended winglet. Thus, there is more lift and less lift induced drag generated.

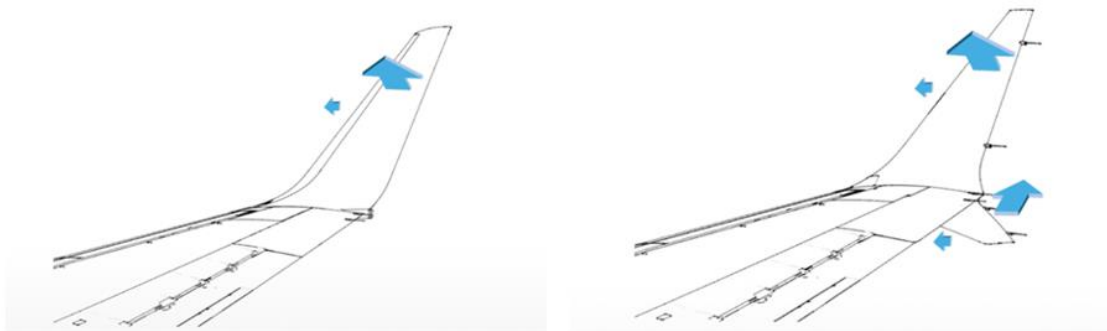


Figure 2.3: Lift vector of split wing tip

With split winglets, the expected reduction of Boeing 737 max in fuel consumption is up to 11.5-13.5% compared to the last model 737 NG that have only 10-12% reduction of fuel consumption (Milic., 2020). Milic., (2020) analysed the aerodynamic performance of the split winglet at 3 different angles of attack at cruising speed of 0.8 Mach in terms of C_L , C_D and compared with the same airfoil of b737c-il wing without winglet. The drag polar in Figure 2.4 showed that the C_L of wing with split

wing tip has increased slightly whilst the C_D of the wing with split wing tip has decreased slightly. The wing with split wing tip has an increase in C_L and its performance.

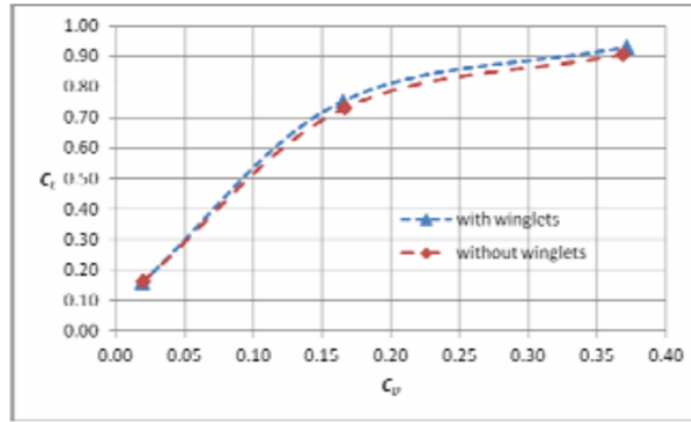


Figure 2.4: Drag polar of wing with and without split wing tip

2.4 Selection of Turbulent Model

To model the fluid flow around the 3D wing, RANS turbulence models comprise of SA model, k-epsilon model and k-omega model were studied. The most suitable RANS turbulence models were employed to simulate the 3D wing at turbulence flow condition of Reynolds number of approximately 13 million. The reason why only the RANS turbulence models are chosen in this study will be presented in Section 3.2.7.

Standard k-epsilon turbulence model

The modelling transport equation for k-epsilon is the turbulence kinetic energy (k) and its dissipation rate (ϵ). The k-epsilon model assumes the flow to be fully turbulent and the molecular viscosity are negligible. The detrimental drawback is the incapability of this model to accurately define the adverse pressure gradients and viscous boundary layer separation. This model usually results in a delay or reduction in separation magnitude. The Enhanced Wall Treatment of k-epsilon is a reinforcement for this model

to determine the flow in the viscous layer. (Villalpando et al., 2011) The k-epsilon model is not generally established for external flow.

Spalart-Allmaras turbulence model

This is a simple one equation model to simplify the free stream and wall boundary conditions of turbulent flow. This model was designed for aerospace flow condition and display good results for boundary layer flow and adverse pressure gradient. However, this model is still relatively new if compare with k-epsilon and k-omega turbulence model. Hence, there is a doubt regarding its suitability for complex flow. (Dash, 2016)

SST k-omega turbulence model

It is a two transport equations model. There is an improvement in this solver model that makes it more reliable than both the k-omega and k-epsilon model as the SST formulation combines both the k-omega and k-epsilon model. This model is ensured to behave properly and accurately in both near wall and far-field zone. There is a development done to enhance the adverse pressure flow and make this model exceptional preferable to predict adverse pressure gradient and flow separation. It is typically more accurate to predict the viscous boundary layer than Spalart-Allmaras model. (Arianzhad, 2015)

Fluent Inc, (2001) stated that the major difference between SST k-omega model and the standard k-omega model is the SST k-omega model utilized the standard model in the boundary layer near the wall surface but experienced gradually change to the high Reynolds number version of k-epsilon model in the outer boundary layer region. There is a cross-diffusion term in the equation of SST k-omega model to guarantee the model acted well in both near wall and outer boundary layer zones. The SST model uses the

low-Reynolds formulation in the boundary layer viscous region and automatic wall treatment is utilized when the cell wall y^+ is around the log-law layer ($20 < y^+ < 300$).

From the studies and findings previously stated above, it is justified that the SST k - ω turbulence model is specifically for wall bounded flow. The SST k - ω model appears to be a better model than the other two turbulence models as it is more suitable in terms of its strength to capture the condition of boundary layer flow, adverse pressure gradient and flow separation. The boundary layer flow is very important to be captured in this case as the flow separation in the boundary layer will provide the precise lift and drag coefficients. This selection of turbulence model comprehended the suitability of the solver model to capture the exact flow pattern around the 3D wing.

2.5 Design of Proposed Wing Tip Device

To initialize the starting of the proposed wing tip device design, the wing tip device designs in the past are studied and gathered to be analysed. The reasonable justification on the proposed design is remarked in this section based on the literature review of previous study carried out. The final proposed wing tip device design is a blended split wing tip design with a smooth chord transition in the area of connection between the wing and both upper and lower winglet as illustrated in Appendix A.

When looked more closely, it is observed that the split wing tip of Boeing 737 max is a combination of the upper and lower canted winglet. The upper canted winglet has a cant angle of 55° and the lower canted winglet has a cant angle of 35° . Gongzhang & Axtelius, (2020) stated that canted winglet integrated into the wing produced an improvement of 4% in lift to drag ratio. Whereas the blended winglet improved the lift to drag ratio by approximately 9% and reduced fuel burn by 4-5%.

Figure 2.5 illustrated a number of wing configurations with and without wing tip devices. The ideal induced drag for each configuration is shown in ascending order. It is clear to visualize that any retreat from the corners of the box increased the ideal induced drag according to Trefftz-plane theory. However, there are viscous drag penalty to be taken into account when there are sharp-cornered intersections. For instances, the blended winglet may have a higher ideal induced drag than the box biplane but the viscous drag is lower (Lean, 2005). From the hypothesis of Trefftz-plane theory above, it is acknowledged that blended winglet has an ideal induced drag of 84.8% when compared to a planar wing even two of its edges retreated from the corners of the box. It is presumed that if a blended split wing tip is created, the wing tip device will have all its tip touching the corner of the box. This will lead to a lower ideal induced drag than the blended winglet according to Trefftz-plane theory. Thus, the proposed design is expected to have a lower induced drag than the split wing tip design in Figure 2.5.

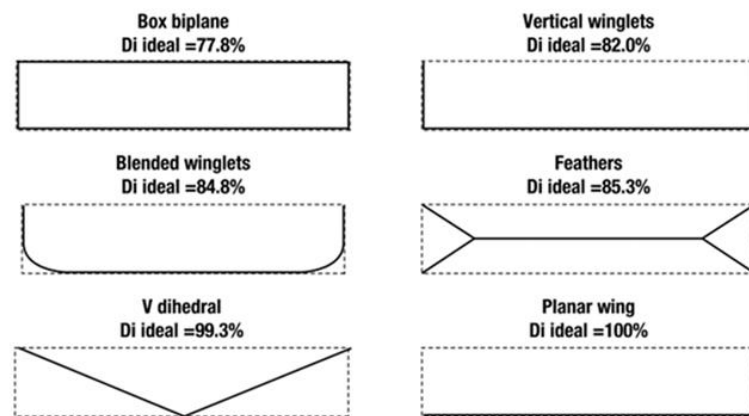


Figure 2.5: Induced drag of several wing lifting surface according to Trefftz-plane theory

In another perspective, the wing winglet intersection with a sharp corner may produce some sort of corner flow. At the rear part of both the main wing and the winglet, the boundary layer at the wing winglet intersection is subjected to an adverse streamwise pressure gradient. This phenomenon exacerbates the flow separation and the drag

(viscous and profile drag) by intensifying the effect of adverse pressure gradient. Adverse pressure gradient being more pronounced is the reversal of flow and the separation of boundary layer. However, the effect of flow separation and the drag can be avoided by using a blended winglet. (Houghton & Carpenter, 2012)

Figure 2.6 shows the streamwise pressure distributions over the upper surface of the wing for different winglet configurations. By observing the (a) and (b) lines from the figure, a pressure distribution with a narrow suction peak followed by a steep adverse pressure gradient close to the wing root is observed. This pressure distribution shows sharp corner wing winglet transition tends to have flow separation. In contrast, the blended winglet has a gentle pressure distribution. (Houghton & Carpenter, 2012) This gentle pressure distribution is more likely to create an elliptical wing loading and have a lower induced drag. Houghton & Carpenter, (2012) clarified that the split wing tip with smooth chord transition with blended winglet has a lower viscous and profile drag. Thus, the study is worth to be carried out to analyse its aerodynamic performance.

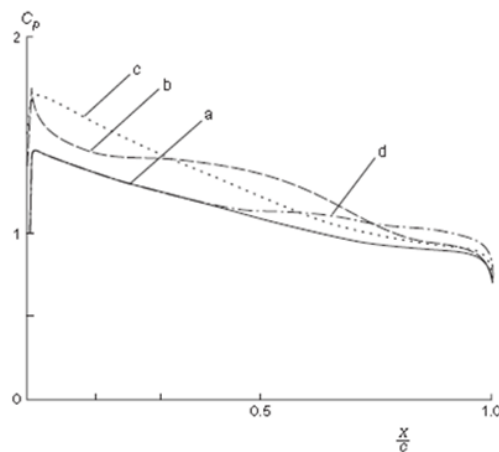


Figure 2.6: The streamwise pressure distributions over the upper surface of the wing for different winglet configurations: (a) wingtip without winglet, (b) winglet with sharp corner, (c) blended winglet

The cant angle of the winglet on the other hand can affect the aerodynamic performance of the wing. Abdelghany et al., (2016) conducted a CFD analysis to study

the effect of winglet cant angle on the performance of the wing. Figure 2.7 showed that when the winglet cant angle is at 45° (purple line) the lift to drag coefficient is highest among all followed by 60° (green line). However, the lift to drag coefficient between winglet cant angle of 60° to 45° does not show much difference. Hence, we can model the proposed split wing tip to have a cant angle between 45° and 60° before blended with a smooth chord transition to optimize the performance of the proposed split wing tip design. The cant angle of the proposed split wing tip is 56.3° before blended. All these findings will be a nascence of design idea for the proposed wing tip design.

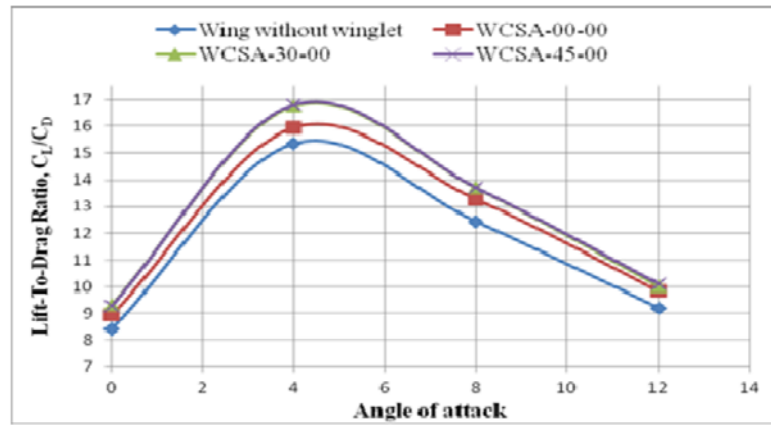


Figure 2.7: Effect of winglet cant angle on lift to drag ratio

2.6 Fluid-Structure Interaction

Fluid-structure interaction (FSI) is the interaction between fluid and structure where the shape of the structure is changed or deformed when there is an internal or surrounding fluid flow (Vigneshwaran et al., 2017). The direct interaction of the deformable wing with the surrounding fluid is called fluid structure-interaction (Ali et al., 2018). Fluid-structure interaction is crucial to the study of deformation of wing structure. It should be realized that the wing is not a rigid structure but a deformable structure. The difference in pressure distribution created by the upper wing surface and

lower wing surface generated some sort of lift distribution loading on the wing structure. This wing structure may deform when they are surrounded by high-speed airflow.

Fluid-structure interaction studies the fluid pressure load and the deformation on the wing structure when fluid flow through it. The fluid flow around a wing varies as the wing structure deform and leads to changes in aerodynamic forces. Hence, fluid-structure analysis is a more precise way to study the aerodynamic performance of a wing structure integrated with a wing tip device.

Basically, a fluid-structure interaction system can be categorized into strong and weak coupled interaction. FSI of weak coupled flow interaction claims that a structure in the flow field only deforms slightly. On the other hand, there is an alteration in the flow field due to the large deformation of the structure in FSI of strongly coupled interaction. Mostly, fluid-structure interaction analysis is solved using numerical simulation tools like ANSYS MECHANICAL since solving analytically is too complex and tedious (Vigneshwaran et al., 2017). Vigneshwaran et al., (2017) solved his aircraft wing by one way coupled FSI. The results of the simulation are there is minimum deformation at the wing root and maximum deformation at the wing tip at all Mach number values.

There are two approaches to solve the FSI problem using numerical simulation tools namely monolithic approach and partitioned approach. The Monolithic approach solved fluid and structure governing equations simultaneously using a unified algorithm solver. This method is more accurate for a multi-physics problem, but it needs more computational memory. In the partition approach, fluid and structure solver are consider as 2 sub solvers. The governing equation of fluid and structure solve separately with different algorithm and boundary conditions. The fluid and the structure program are

solved individually according to 2 different mesh. The benefit is the computational time is reduced (Ahamed et al., 2017)

In FSI, one-way coupling is utilized when the structure deformation is affected by the fluid flow and vice versa. Whereas two-way coupling is applied when structural deformation is affected by fluid flow and concurrently fluid flow is affected by structural deformation as well. Both of these methods are based on the partition approach where this two structure and fluid field have their own solver but the information is exchanged between these solvers (Ahamed et al., 2017). In this research, one-way coupling FSI is sufficient for the study. This is solely because the deflection of a wing affected by the pressure loadings will change the flow field and pressure distribution, but the changes are negligible. Hence, for simplicity after solved with the structure solver the geometry change is unnecessary to solve by the fluid solver.

Ishak et al., (2020) stated that the governing equation for structural domain can be obtained from conservation of linear momentum. Ishak et al., (2020) used one-way coupling FSI method to consider the FSI analysis on Aircraft Wing with supersonic and transonic speed. The wing and winglet surfaces will be the interfaces of FSI fluid and structure domains. There are several coupling boundary conditions applied to couple the fluid and structure domains. The coupling boundary conditions are kinematic coupling of fluid and structure velocities and dynamic coupling of balance forces contacts.

CHAPTER 3

METHODOLOGY

3.1 Overview

In preparation for facilitating the research to reach the objectives, the aerodynamic aspects of wing tip and its performance was first studied and investigated. Subsequently, the literature findings of the studies were discussed in Chapter 2 Literature Review. Thereafter, the proposed design was drawn based on the literature findings of existing wing tip devices. The suitable solver for the 3D model is then investigated and studied. The most appropriate solver is then chosen between Spalart-Allmaras, K-epsilon and K-omega.

Hereafter, the meshing setup and the suitable solver model is then validated in the 3D case by designing a NACA 4412 rectangular wing and compared the simulation results with the previous research carried out by Petinrin & Onoja, (2017). The aerodynamic performance (coefficient of lift and drag) analysis on different Mach number and angle of attack will be performed on the 3D wings by the validated meshing setup and solver setup using ANSYS Fluent simulation. The coefficient of lift and drag is studied as these two aspects is the core of aerodynamic and are simple to compare between each wing. After the aerodynamic analysis, the FSI analysis is carried on to study the structural response of the 3D wing models when the fluid flow pressure acts on the solid surface.

FSI is used to link between the fluid and structure solver and the coupling in this research work is based on one-way coupling FSI. In one way coupling FSI, the fluid flow is calculated in the fluid domain and the resulted flow field pressure is transferred to the structural domain to carry out the solving process up to convergence. Subsequently, the

FSI for the next time step will be carried out until stopping criterion was met. In the FSI analysis, Aluminium alloy material was selected on all the 3D wing models as it is the commonly used material for aircraft wing. The structural response was then compared between the 3 wing models.

Two-way coupled FSI is needless in this case because the fluid and solid solutions are weakly coupled in this research. The overall project flow chart and one-way coupling FSI chart are illustrated graphically as shown in Figure 3.1 and Figure 3.2.

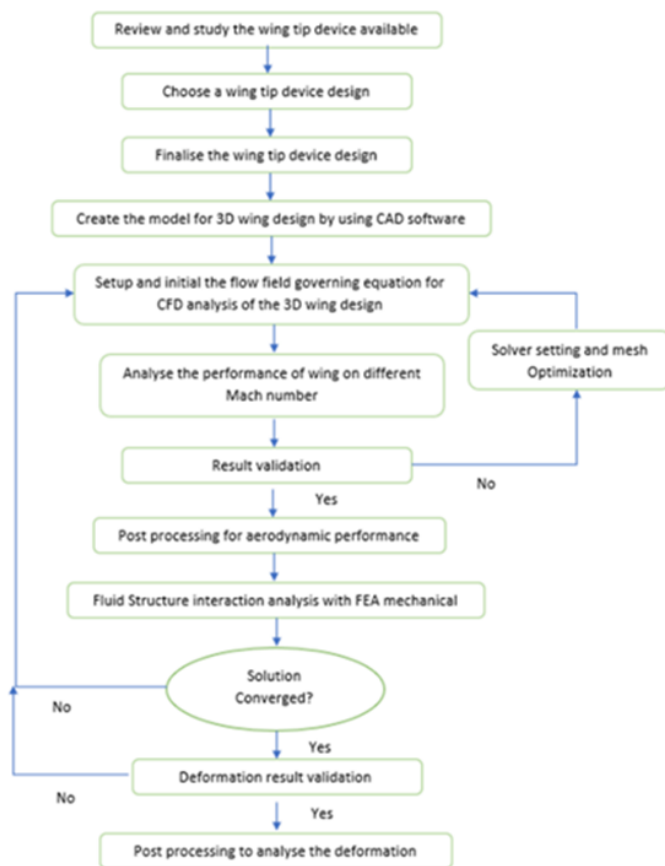


Figure 3.1: Overall project flow chart

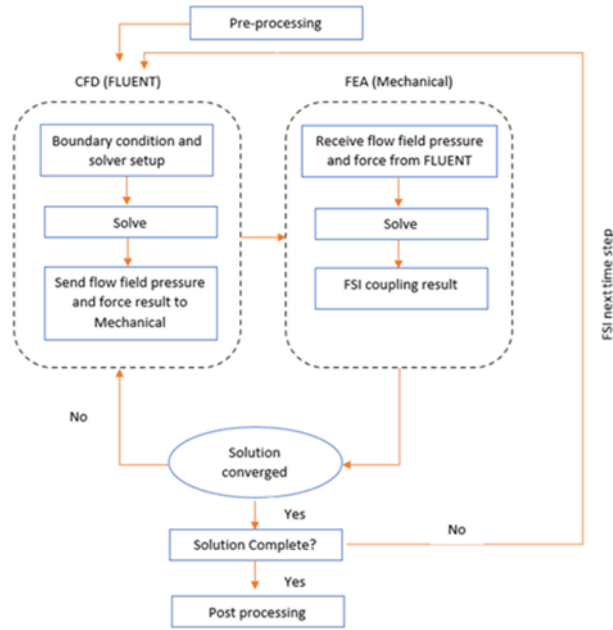


Figure 3.2: Flow chart of one-way coupling FSI

3.2 3D Aerodynamic Analysis

In this thesis, the analysis of three 3D wing design is carried to determine their aerodynamic performance. The three wings designs are wing with no wing tip device, wing with split wing tip and wing with blended split wing tip. These three wings are designed with 2D Boeing b737c-il airfoil. The study of aerodynamic performances of lift and drag at different Mach number and angle of attack is the primary concern. These key features are the main focus as the fuel efficiency of the aircraft is depending on lift and drag. Since the Boeing 737 max aircraft is a civil commercial aircraft, the aerodynamic analysis will only cover the subsonic and transonic flow from 0 to 16 angle of attack.

3.2.1 3D Wing Model CAD Design

The SOLIDWORKS CAD 2020 software was utilized to design the geometric model of Boeing 737 max split wing tip design, proposed blended split wing tip design and a dummy model of wing with no wing tip device. The conceptual design of the

proposed split wing tip design was modelled based on the finding and justification obtained from the literature review of wing tip devices design in Chapter 2. Split wingtip claimed to reduce fuel burn by 1.5% and drag up to 9.5% as well when compared to an unmodified wing (Gongzhang & Axtelius, 2020). The Boeing 737 max split wing tip design and the dummy model is imitated from the limited source available online. In this research, aerodynamic performance was the main concern. The conceptual design was initiated by taking aerodynamic performance into consideration and without concern for the manufacturing and fabrication process.

The designing process is first started with importing the different chord of airfoil b737c-il profiles in specific location pre-determined. Those specific locations were the root, mid span, tip and wing tip. Meanwhile, for the dummy model of wing with no wing tip device only root, midspan and tip profile are needed in the designing process.

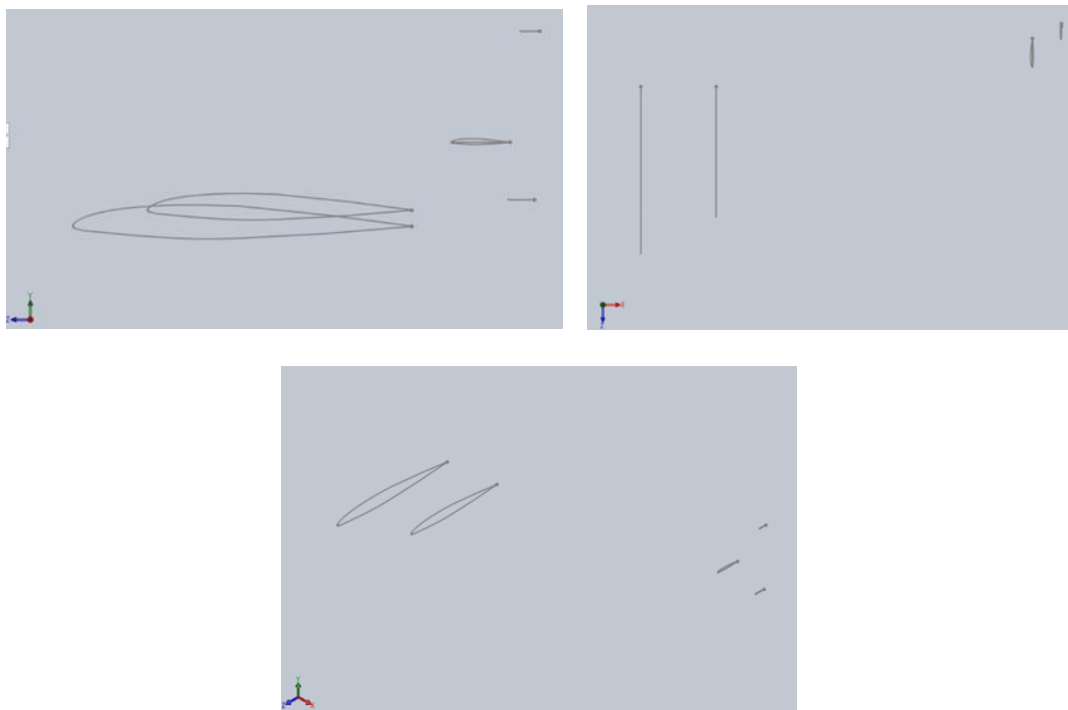


Figure 3.3: The side, top and isometric view of airfoil profile at specific location for 3D wing design

The conceptual designs of the split wing tip and wing without wing tip were designed based on the airfoil profiles as shown in Figure 3.3. These 2 wing designs are depicted in Figure 3.4 and Figure 3.5.

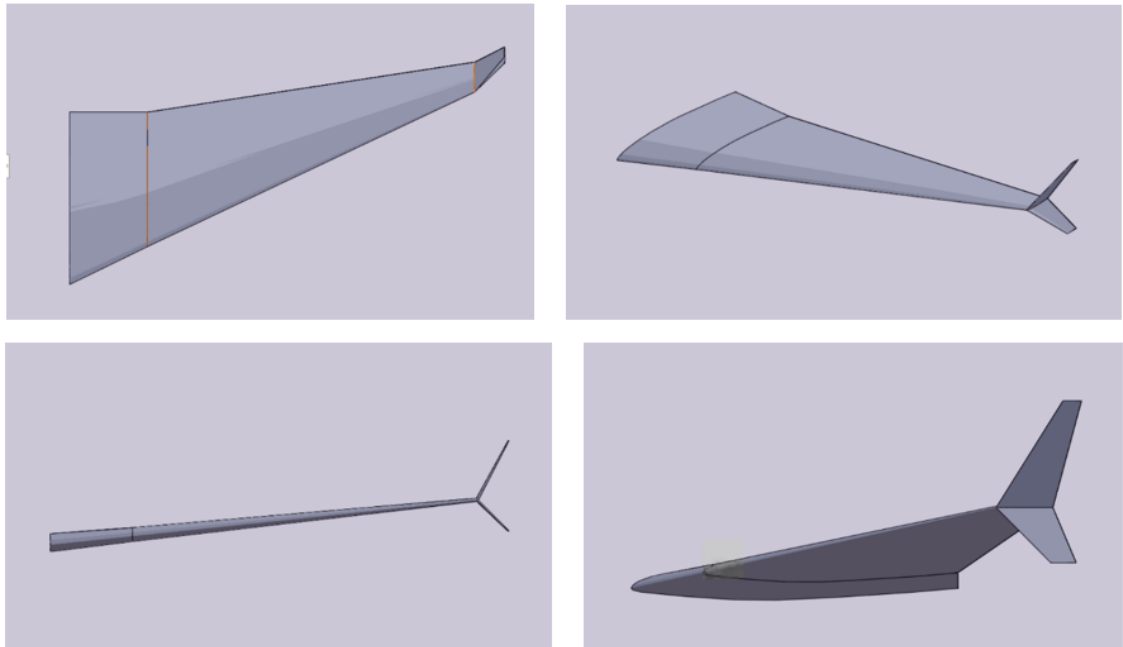


Figure 3.4: Top, isometric, front and side view of split wing tip wing design

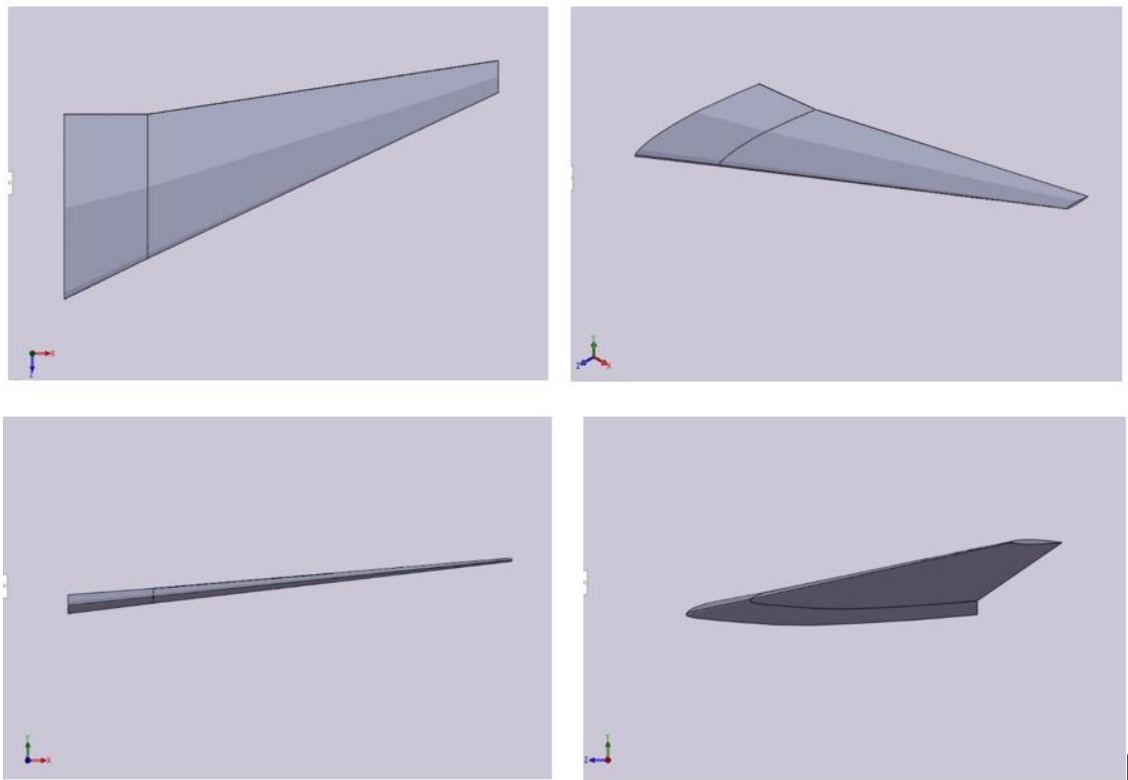


Figure 3.5: Top, isometric, front and side view of wing design with no wing tip

The proposed conceptual blended split wing tip design of the 3d wing model was optimized and illustrated in Figure 3.7. The proposed design was inspired by the blended wing design and split wing tip design of Boeing 737 max and examined upon reaching the best design. The design was finalized after performing reasonable justification based on the literature review of previous study. The cant angle of the wing tip is ensured to be in the range between 45° and 60° before blended with smooth chord transition to enhance the aerodynamic performance. The 3D model was designed based on the specific location of root, mid span, tip and wing tip profile guided by guidelines depicted in Figure 3.6. Detail drawings of the 3D wing model designs are attached in Appendix A.

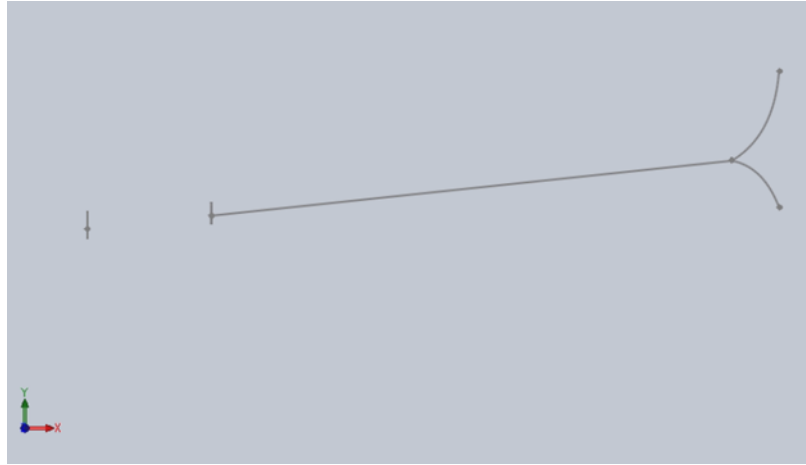


Figure 3.6: Guidelines for blended split wing tip design

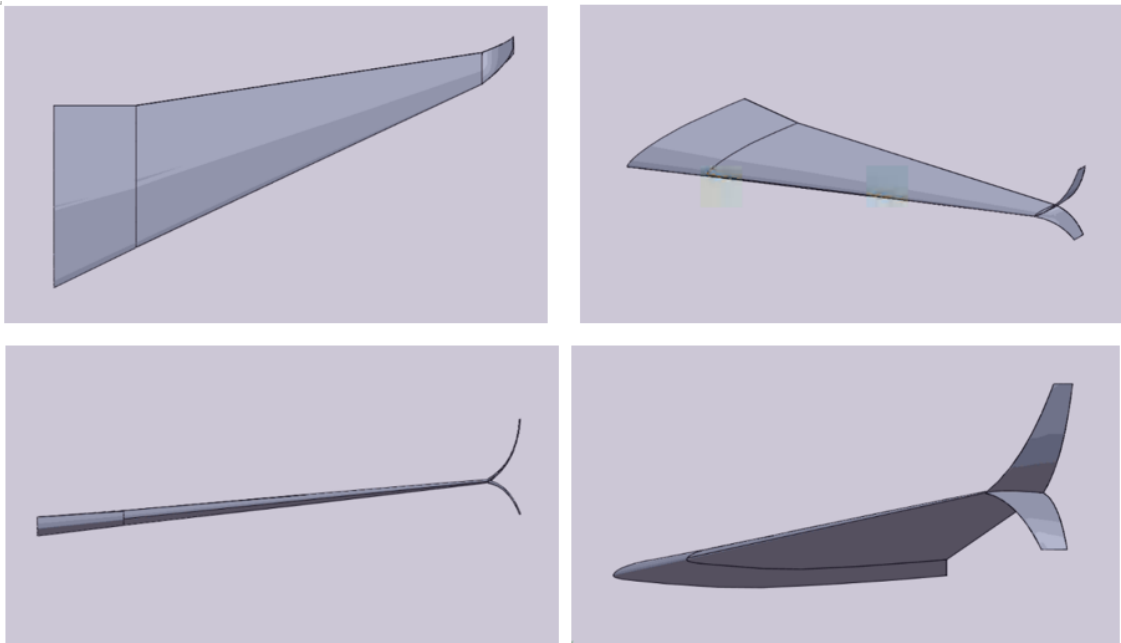


Figure 3.7: Top, isometric, front and side view of blended split wing tip wing design

3.2.2 Design Parameter of 3D Wing

The 2D airfoil for all the wing design is b737c-il. This airfoil shape is obtained from airfoil tools website and imported to SOLIDWORKS to design the wing. The b737c-il airfoil is used by all of the Boeing 737 family aircraft. Some of the basic parameters are shown in Table 3.1. Most of the basic design parameter is obtained from